Pure Appl. Geophys. 181 (2024), 2131–2147

https://doi.org/10.1007/s00024-024-03510-3

Pure and Applied Geophysics

Estimation of Pore Structure for Heterogeneous Reservoirs Based on the Theory of Differential Poroelasticity

Jing Ba,[1] Zhijiang Ai,[1] José M. Carcione,[1,3] Mengqiang Pang,[1] Xinfei Yan,[2] and Xiao Chen[4]

Abstract—The complex seismic responses of heterogeneous reservoirs can be related to the fabric structure, pore/microcrack shape, mineral composition and fluid distribution of the rock in situ. The pore structure refers to the geometric shape, size, spatial distribution and interconnectedness of pores, microcracks and throats. It is closely related to the storage space of reservoirs and the spatial distribution of oil/gas. Understanding the pore structure is crucial for the development of processes to increase oil/gas production capacity. Six dolomite samples from the Gaoshiti-Moxi Longwangmiao Formation are sorted out for measurements, and the ultrasonic and seismic attenuation are determined by using the spectral ratio method and the enhanced frequency shift method, respectively. When predicting the pore structure, we assume that the aspect ratio and volume fraction of pores and microcracks correspond to a normal distribution. On this basis, a model with the Voigt–Reuss–Hill average (VRH), differential effective medium (DEM) theory and infinituple-porosity media (IPM) theory is proposed. The acoustic wave responses in terms of reservoir porosity and standard deviation of normal distribution are analyzed, and multiscale 3D rock physics templates (RPT) are created. The calibrations of the templates are performed with the ultrasonic and seismic data, and then the templates are applied to the field data. The results show that the estimated porosity and pore structure (corresponding to the mean aspect ratio and standard deviation of a normal distribution, respectively) are in substantial agreement with the log data and the actual gas production results.

Keywords: Dolomite reservoir, pore structure estimation, attenuation, rock-physics template, infinituple-porosity media theory.

1. Introduction

With the depletion of conventional oil/gas reservoirs, the main target of seismic exploration has gradually shifted to the deep heterogeneous reservoirs in complex geological environments (Ghanizadeh et al., 2015; Li et al., 2020; Liu et al., 2022; Luo et al., 2023; Shi et al., 2021). Carbonate reservoirs are common (Cao et al., 2018; Pang et al., 2019, 2024; Sayers, 2008), and the rocks can be highly heterogeneous due to the presence of microcracks, fractures and troughs (Mousavi et al., 2012; Xu & Payne, 2009). These features can be important for effective oil/gas production in low porosity and permeability reservoirs (Lu et al., 2019; Sun et al., 2019; Zheng et al., 2020). There are difficulties in the characterization of these reservoirs with using conventional petrophysical models and seismic processing/inversion techniques (Zhang et al., 2018; Zhao et al., 2016).

The heterogeneity of rock microstructure affects the petrophysical responses or properties of reservoirs (Amalokwu et al., 2014; Ba et al., 2012; Chapman et al., 2016; Dutilleul et al., 2020; Iwamori et al., 2021; Nie et al., 2012; Solazzi et al., 2019; Zhang et al., 2022). Carcione and Picotti (2006) investigated the effects of heterogeneity in rock porosity, grain and frame moduli, permeability and fluid properties on wave attenuation and velocity dispersion. Fu et al. (2018) analyzed the influences of crack density and geometry on elastic wave dispersion and attenuation under high- and low-frequency conditions. Sun et al. (2019) used computed tomography (CT) to create three-dimensional digital rock cores and analyzed how microfractures affect fluid flow in tight reservoirs, finding that the microfracture aperture has the

[1] School of Earth Sciences and Engineering, Hohai University, Nanjing 211100, China. E-mail: jba@hhu.edu.cn
[2] Research Institute of Petroleum Exploration and Development, PetroChina, Beijing 100083, China.
[3] National Institute of Oceanography and Applied Geophysics - OGS, Trieste, Italy.
[4] Research Institute of Exploration and Development, Southwest Oil & Gas Field Company, PetroChina, Chengdu 610041, China.

greatest influence. Wang et al. (2020) used a combination of Bayes discriminants and deterministic rock physics modeling methods to achieve joint probabilistic fluid discrimination in tight sandstone reservoirs. Wei et al. (2021) analyzed the effects of rock permeability and fluid saturation on the dispersion and attenuation properties of seismic waves in partially saturated sandstones.

The spatial distribution of pores and microcracks have been considered a critical factor in hydrocarbon reservoir exploration and production (Ba et al., 2011; Benaafi et al., 2019; Fang et al., 2019; Hu et al., 2020; Kong et al., 2018; Nelson, 2001; Sanderson & Nixon, 2015; Zhao et al., 2020). Ba et al. (2017) proposed a double double-porosity (DDP) theory that considers the overlapping effect of double porosity and patchy saturation. Guo et al. (2021) established three rock physics models to describe the elastic wave responses of heterogeneous pore structures in tight sandstones, evaluated the applicability of the models, and used a normal distribution to represent the pore structures. Zhang et al. (2021) developed a theory of wave propagation in a fluid-saturated medium with infinite porosity phases and inclusions at multiple scales based on the differential effective medium (DEM) theory for a solid composite and the Biot-Rayleigh theory for the anelasticity of a double-porosity medium. Zhang et al. (2022) extended the theory to the case of a partially saturated medium and proposed a modeling approach to describe the anelastic waves transmitting in rocks with a fractal distribution of fluid patch scales.

Core samples of dolomites from the Gaoshiti-Moxi area are collected to analyze the pore structure and mineralogy by using X-ray diffraction tests (XRD) tests, thin sections (CTS) and ultrasonic tests at different pressures. The spectral ratio method and the frequency shift method are used to estimate ultrasonic and seismic attenuation, respectively. The VRH, DEM and IPM theories are used to calculate the P-wave attenuation, P-wave impedance and P- and S-wave velocity ratio (V_P /V_S), and generate multiscale 3D RPTs for the dolomites. The pore structures are represented with a normal distribution and the reservoir porosity and pore structure are related to the seismic responses. The templates are calibrated with the ultrasonic and seismic data. Then, the seismic data of the working area is used to predict the porosity and pore structure of the reservoirs.

2. Reservoir Characteristics

2.1. Geological Setting

For the tight gas reservoirs of the Longwangmiao Formation in the Gaoshiti-Moxi area, Sichuan Basin, the predominant mineral component is dolomite. The Gaoshiti-Moxi area is located in the central Sichuan Basin and covers an area of around 5288 km^2. The Sichuan Basin has experienced several tectonic changes that have led to different phases of structural unconformities. The depth of the Longwangmiao Formation can be more than 4 km and is influenced by an ancient landform. Overall, it has a west-thin and east-thick structure, representing the sedimentation of the carbonate platform. The thickness of the Longwangmiao Formation in the Gaoshti area is 80–100 m, with an average thickness of 93.8 m, and the thickness gradually increases from east to west and from south to north (Fan et al., 2021; Zhang et al., 2015).

The reservoir rocks are mainly granular and crystalline dolomites with vugs and intergranular/intercrystalline pores. The diagenesis of the Longwangmiao Formation reservoirs in the Gaoshiti area is controlled by the sedimentary facies, and their vertical development and lateral distribution are affected by the sub-facies of the granular shoals. Large areas of the granular shoals are formed with tight rocks and strong heterogeneity. The average porosity is 4.24%. The cumulative thickness of the reservoirs range between 2.9 and 35.0 m (Fan et al., 2021; Yang et al., 2015; Zhang et al., 2015). The immiscible fluids (gas and water) are heterogeneously distributed within the pores and the microcrack system (Pang et al., 2019).

2.2. Core Samples

Four dolomite samples (S1–S4) are taken from well A, formed into cylinders with a diameter of 37.9 mm and a length of 50 mm (see Table 1). X-ray diffraction tests (XRD) and thin section analyses

Table 1

Rock-sample properties

Sample	S1	S2	S3	S4	A1	A2
Porosity (%)	1.96	2.81	2.46	3.46	5.10	5.34
Permeability (mD)	0.159	0.141	0.135	0.001	0.091	0.458
Density (g/cm^3)	2.798	2.753	2.761	2.743	2.69	2.66

(CTS) are carried out to analyze the mineralogy and pore structure. The minerals are mainly dolomite, which accounts for more than 98% by volume, as well as a small amount of calcite, clay and other minerals. Figure 1 shows the thin sections of samples S1 and S4, in which the pore space consists of intergranular pores and microcracks. The porosity is mainly in the range of 1–5% and the permeability is 0.001–0.2 md, with poor pore connectivity. Two additional pure dolomite samples from the Tarim Basin (A1 and A2) are also considered, which have similar lithologic and physical properties to samples S1–S4.

3. Experimental Tests and Data Analysis

3.1. Ultrasonic Measurements

Measurements of the ultrasonic wave velocities are carried out on the water-saturated dolomite samples at different differential pressures. The samples are dried in an oven and then saturated with water. Each sample is sealed with a rubber sleeve and placed in the experimental setup (Guo et al., 2009), which allows the confining pressure and pore pressure to be controlled. The pore pressure is fixed at 15 MPa, and confining pressures of 20, 25, 30, 35, 40, 45, 50 and 55 MPa are applied. At each confining pressure, the waveforms transmitting through the rock are recorded.

Figure 2 shows the P- and S-wave velocities of the six samples as a function of differential pressure. It can be seen that V_P and V_S of saturated dolomites gradually increase with pressure. As pressure increases, the pores and microcracks gradually ten to close, leading to an increase in the elastic moduli and higher velocities. In the six dolomites, the samples with relatively high porosities have lower velocities. As the differential pressure increases, the slope of V_P (V_S) with respect to the pressure decreases.

Figures 3 shows the velocities as a function of porosity for the 6 dolomites at full water saturation. In general, both velocities decrease with increasing porosity. A lower porosity may correspond to higher bulk and shear moduli.

The spectral-ratio method is adopted to estimate the wave attenuation (reciprocal of the quality factor,

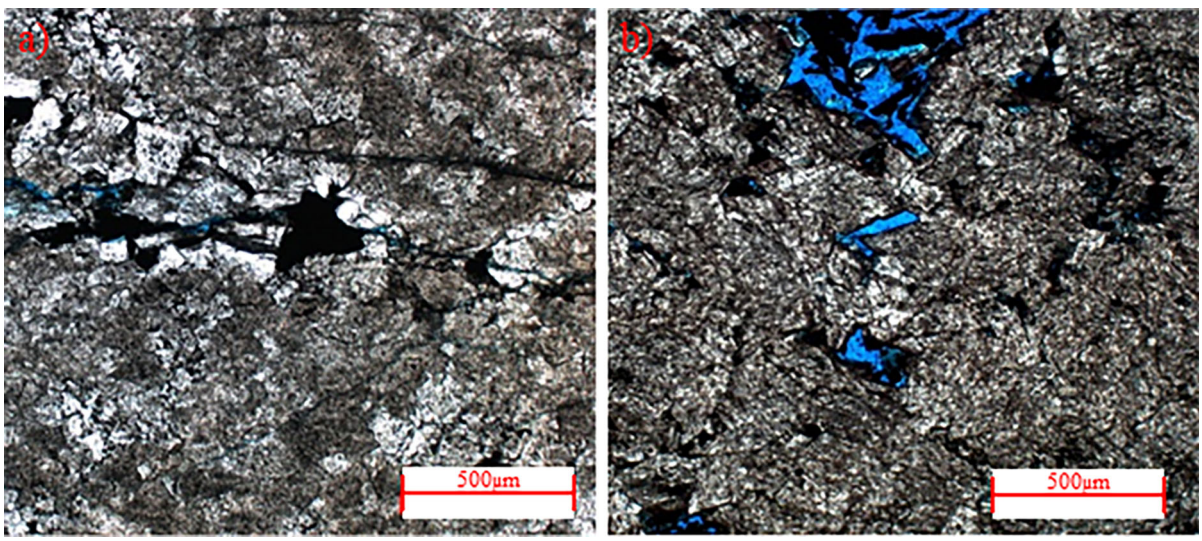

Figure 1
Thin sections of samples S1 (**a**) and S4 (**b**)

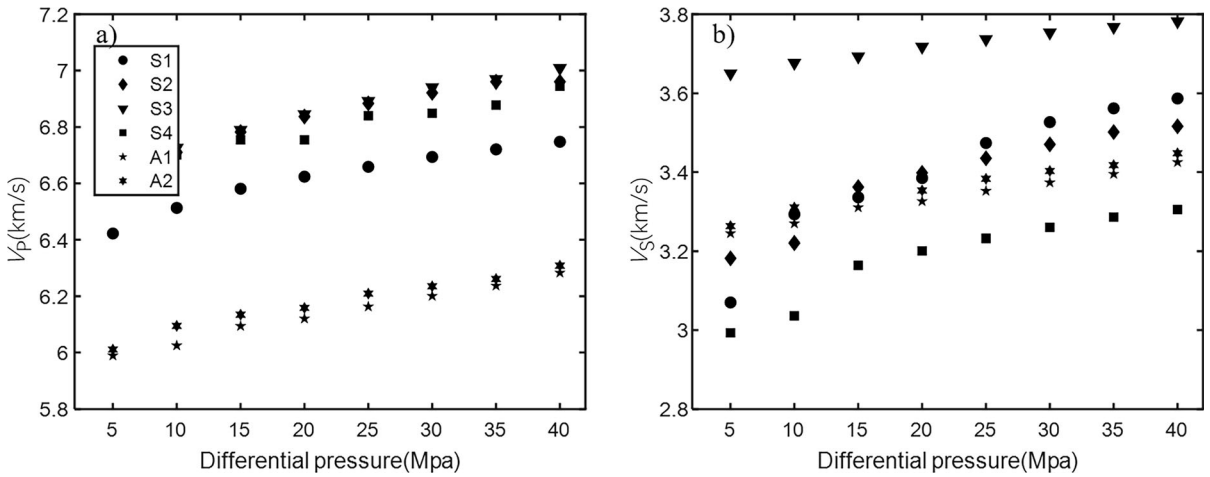

Figure 2
P-wave (**a**) and S-wave (**b**) velocities as a function of differential pressure for the 6 dolomites at full water saturation

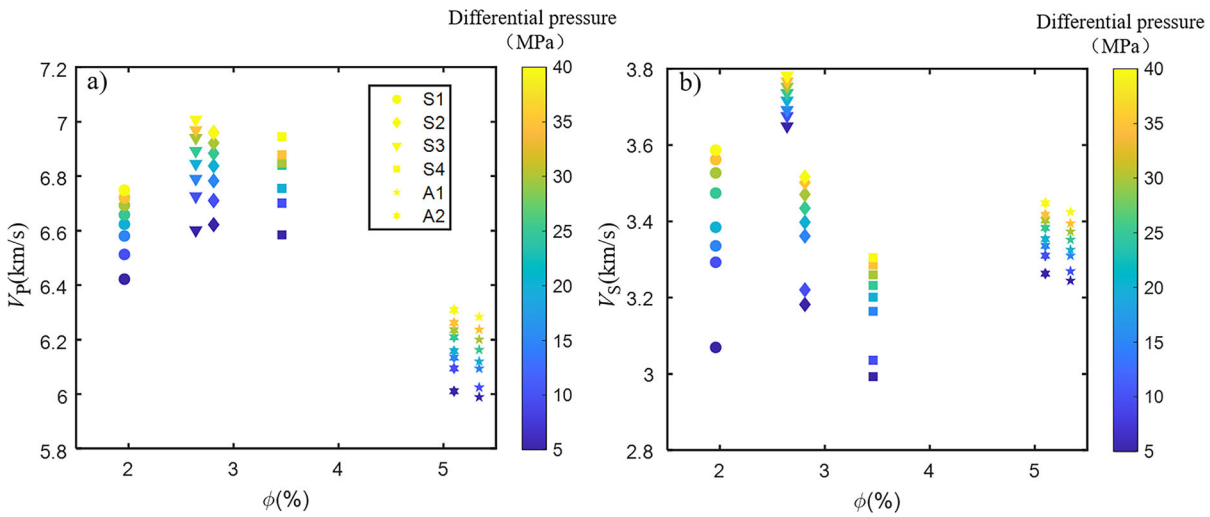

Figure 3
P-wave (**a**) and S-wave (**b**) velocities as a function of porosity and differential pressure for the six samples at full water saturation

1000/Q), by considering the standard aluminum blocks with high quality factors as reference materials (Guo & Fu, 2006; Toksöz et al., 1979).

Figure 4 illustrates the waveforms for the aluminium and the saturated sample. The selected waveform is considered as the time window, indicated with the red bars. The spectral-ratio method is then applied to compute the P-wave attenuation under the different pressures. Figure 5 shows the P-wave attenuation as a function of porosity and differential pressure at the full saturation. The attenuation increases with increasing porosity and decreases with the pressure. An increase in the differential pressure leads to a reduction of the microcrack porosity (Pang et al., 2020; Song et al., 2015) and intrinsic attenuation.

3.2. *Well-Log Data*

The logging curves of V_P, V_S, density (ρ), porosity (ϕ) and saturation (S_w) for the target layer of well B

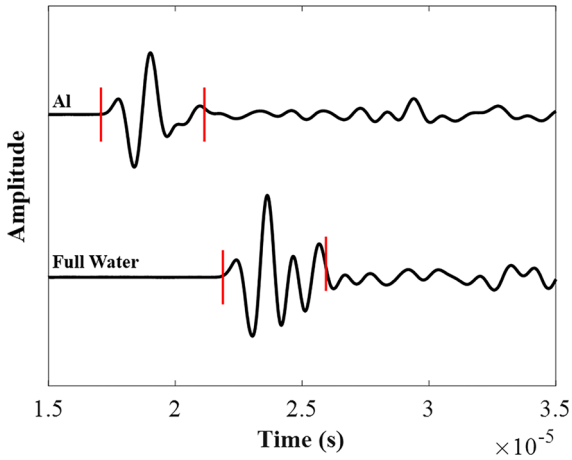

Figure 4
Waveforms for the aluminum and rock sample (sample S1 at 5 MPa) at full water saturation

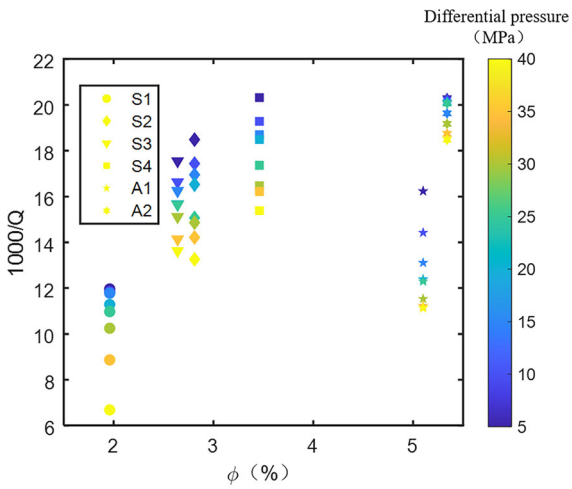

Figure 5
Ultrasonic attenuation as a function of porosity and differential pressure for the 6 samples at full water saturation

in the work area are extracted (Fig. 6). The porosity and gas saturation ($1 - S_w$) in the upper and middle sections for the target layer are relatively high. Figure 7 shows a decreasing trend of velocity with porosity, which ranges between 0 and 5%.

3.3. Seismic Attenuation Estimation

Traditional methods for estimating the attenuation include the peak frequency-shift method and the centroid frequency-shift method. Tu and Lu (2009), Hu et al. (2013) and Li et al. (2015) proposed an extended frequency shift method to estimate seismic attenuation by combining the two methods, with which the estimated Q exhibits a higher precision and can be well applied in the actual seismic data processing.

Figures 8 and 9 show the amplitude and attenuation profiles ($1000/Q$) extracted from lines 1 and 2 in the working area, where line 1 crosses boreholes A and B and line 2 crosses boreholes C and D. It can be seen that a stronger attenuation of the target layer occurs around boreholes B and C.

4. Rock-Physics Model

4.1. Dolomite Reservoirs

We assume that the aspect ratio and volume fraction of pores and microcracks statistically satisfy a normal distribution, where the mean aspect ratio is $\alpha = 10^{-\mu}$, and μ is the mean value, and water is the saturating fluid for rock physics modeling of this study (where patchy saturation is not considered since such a complex structure has been incorporated). The aspect ratio of 0.01 is considered to differentiate the stiffer pores ($\alpha \geq 0.01$) and soft microcracks ($\alpha < 0.01$), as is showed in Fig. 10. With the increase of the mean aspect ratio value, the general aspect ratios of pores and microcracks increase, while the proportion of microcracks decreases. With the increase of the standard deviation for the fixed mean aspect ratio, the dispersion of pore/microcrack aspect ratio increases, while the proportion of microcracks increases as is shown in Fig. 10a.

Figure 11 shows the modeling procedure. The mineral composition of the reservoir rocks is almost pure dolomite and contains a small amount of clay. The content of dolomite is around 98%. The bulk and shear moduli of dolomite and clay are 94.9 and 45 GPa, and 25 and 9 GPa, respectively. First of all, the Voigt–Reuss–Hill (VRH) (Hill, 1952; Reuss, 1929; Voigt, 1910) equation is applied to estimate the elastic moduli of the mineral mixture. Pores are included in the host medium, and microcracks are added into the solid inclusions through DEM. The dry-rock moduli are obtained by mixing the host

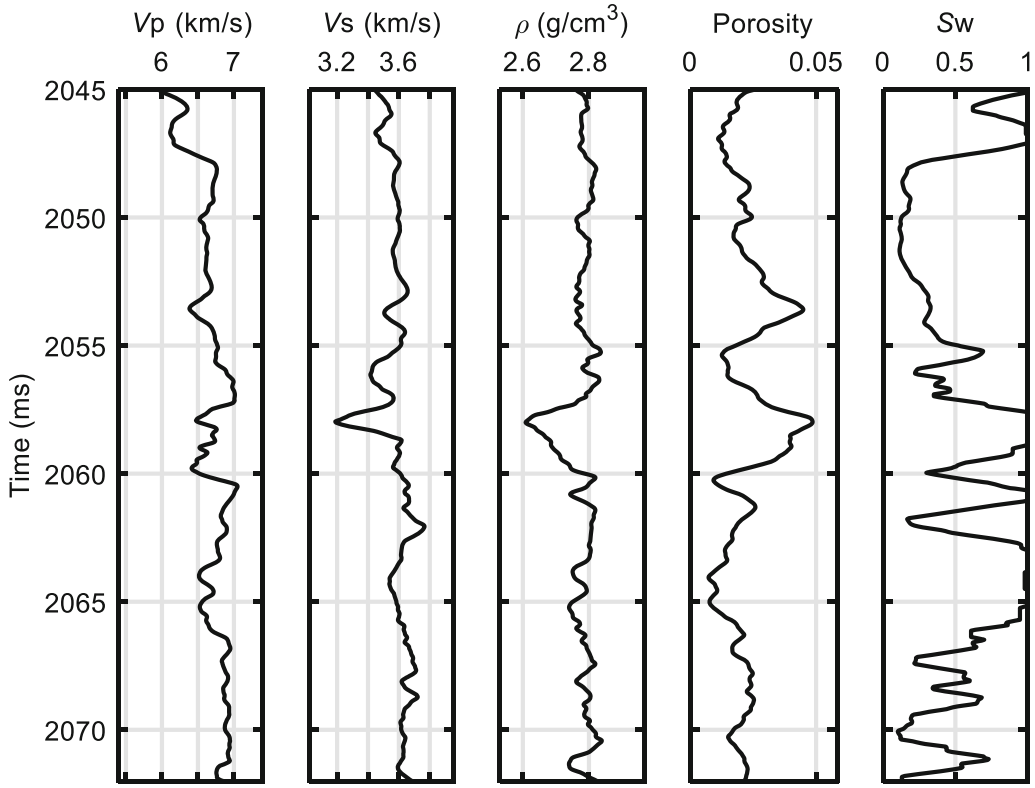

Figure 6
Logging data of the formations corresponding to well B. The columns from left to right represent V_P, V_S, ρ, porosity and Sw

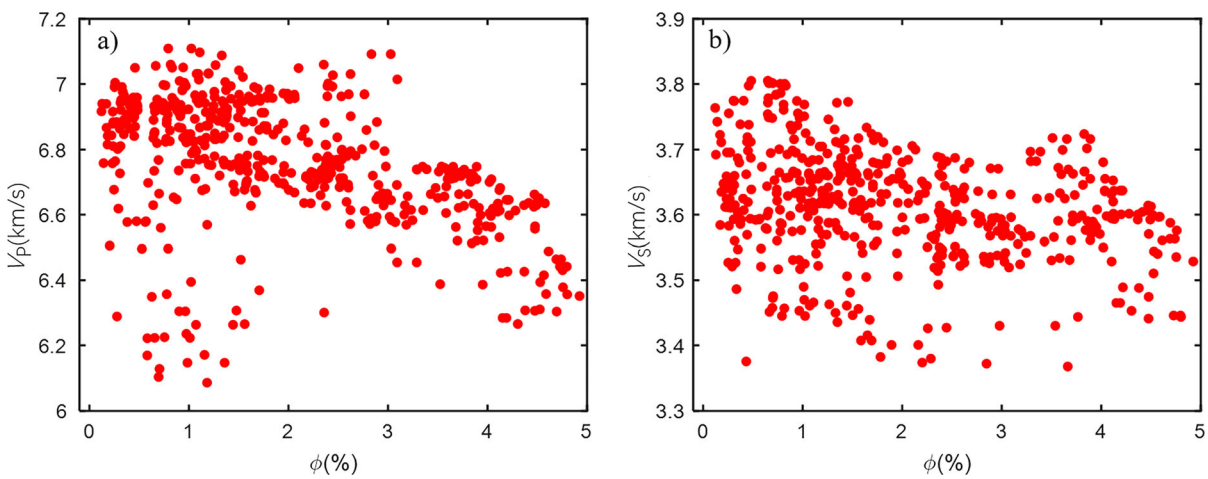

Figure 7
Relation between porosity and V_P (**a**) and V_S (**b**) corresponding to the logging data

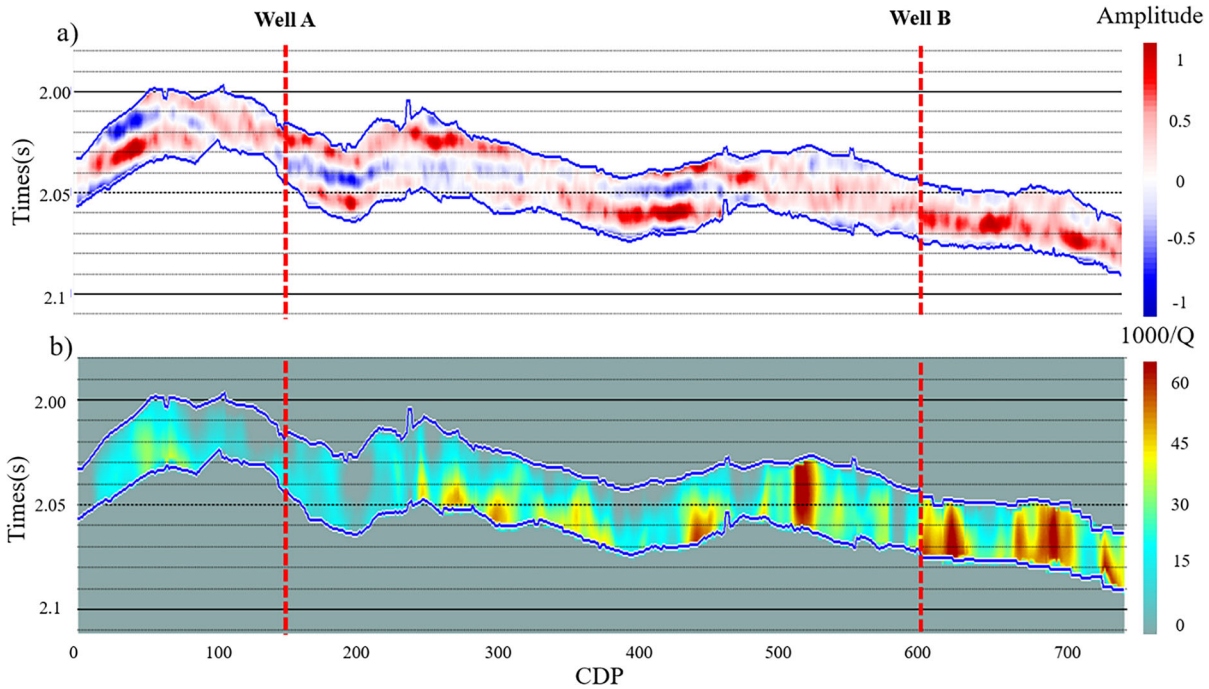

Figure 8
2-D amplitude (**a**) and attenuation (**b**) profiles of line 1 crossing wells A and B

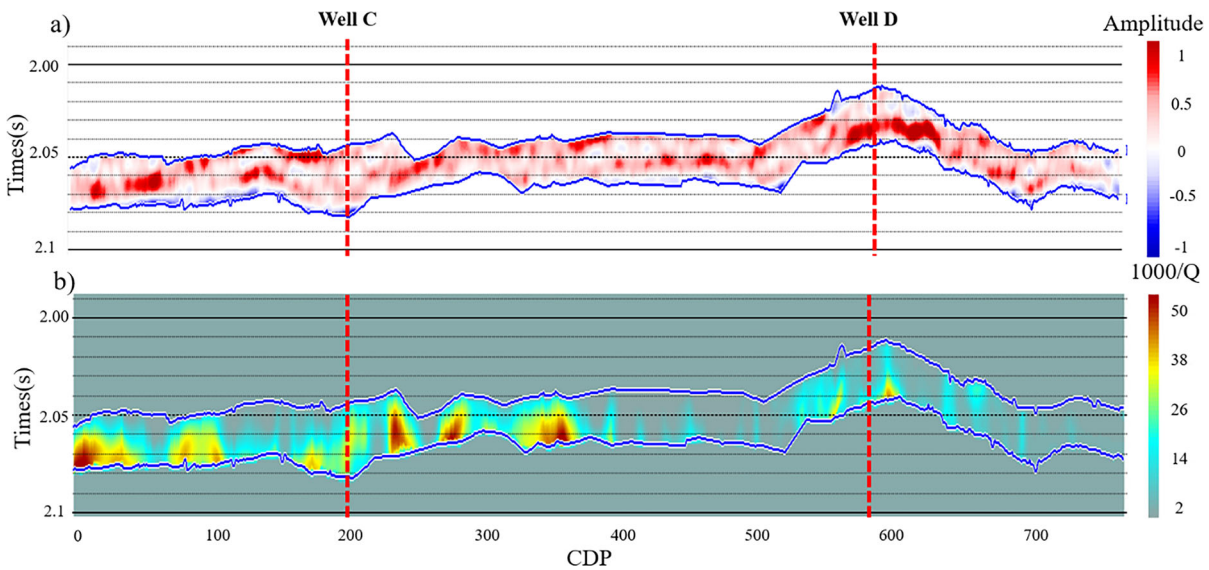

Figure 9
2-D amplitude (**a**) and attenuation (**b**) profiles of line 2 crossing wells C and D

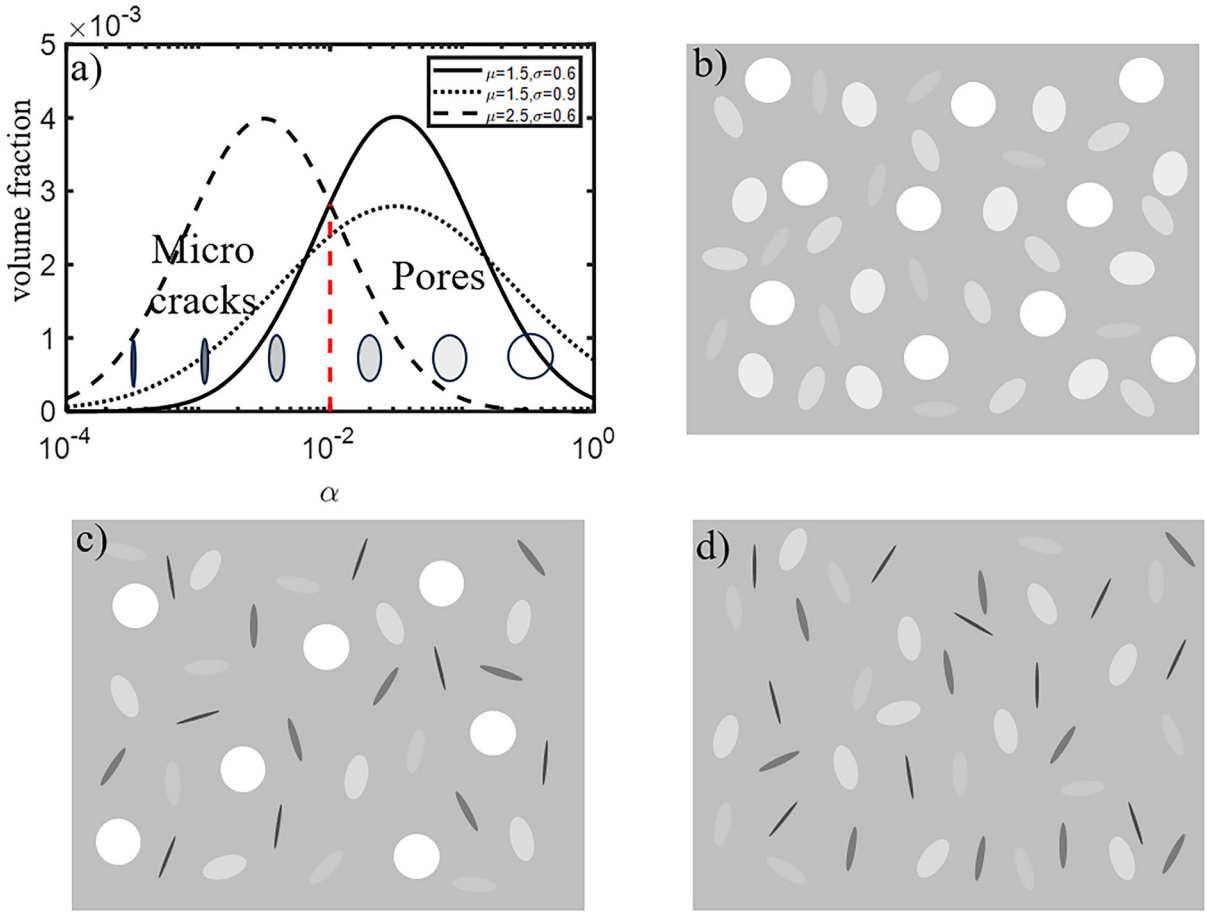

Figure 10
a Effects of the mean and standard deviation of a normal distribution for the system of pores and microcracks, where **b** $\mu = 1.5,\ \sigma = 0.6$, **c** $\mu = 1.5,\ \sigma = 0.9$, and **d** $\mu = 2.5,\ \sigma = 0.6$

medium and the inclusions, based on the DEM equation (Berryman, 1992; Zhang et al., 2021).

Then, the IPM theory is applied (inclusions are added incrementally) for fluid substitution with intergranular pores and sets of microcracks with different shapes (Zhang et al., 2021). The IPM equations are given in Zhang et al. (2021) and Gassmann (1951) equations (Gurevich & Carcione, 2022) are used to compute the wet-rock moduli at the end of each addition, and used as the moduli of the new host medium for the next addition. Gassmann equations are

$$\frac{K_{sat}}{K_0 - K_{sat}} = \frac{K_b}{K_0 - K_b} + \frac{K_f}{(\phi + d\phi)(K_0 - K_f)}, \quad (1a)$$

$$G_b = G_{sat}, \quad (1b)$$

where ϕ is the total porosity, K_0 and K_f are the grain and fluid bulk moduli, K_b and G_b are the dry-rock bulk and shear moduli, and K_{sat} and G_{sat} are the complex bulk and shear moduli of the composite porous medium, respectively.

The final P-wave wavenumber k is obtained at the last iteration, and the phase velocity and quality factor are obtained as (Carcione, 2022)

$$V\mathrm{p} = \left[\mathrm{Re}(v^{-1})\right]^{-1}, \quad (2)$$

and

$$Q = \frac{\mathrm{Re}(v^2)}{\mathrm{Im}(v^2)}, \quad (3)$$

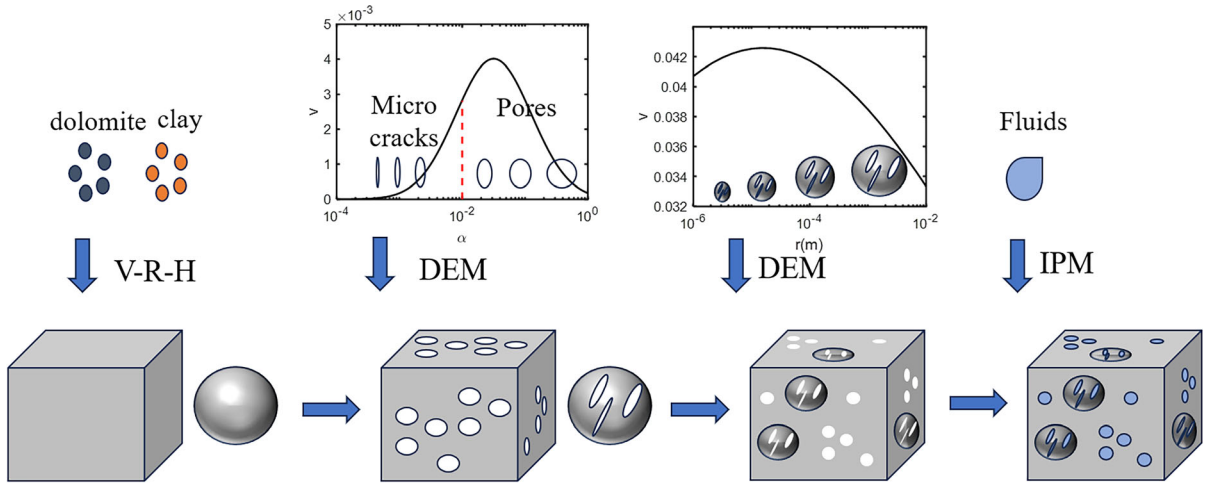

Figure 11
Flowchart of the rock-physics modeling

respectively, where $v = \omega/k$ is the complex velocity and ω is the angular frequency.

4.2. Wave Velocities and Attenuation

The proportions of dolomite and clay are set as 98% and 2%, respectively. Water has a bulk modulus of 2.25 GPa, a density of 0.98 g/cm^3 and a viscosity of 0.001 Pa•s. The properties of the mineral mixture and rock skeleton are computed with the VRH average and DEM equations, respectively. By considering the full water saturation, the P-wave velocity and attenuation of dolomites are obtained as a function of frequency for different total porosities (Fig. 12) and standard deviations (Fig. 13).

Figure 12 shows the velocity and attenuation of the P-wave as a function of frequency and porosity. The mean aspect ratio is set to 0.0316 and the standard deviation to 0.20. The wave dispersion and

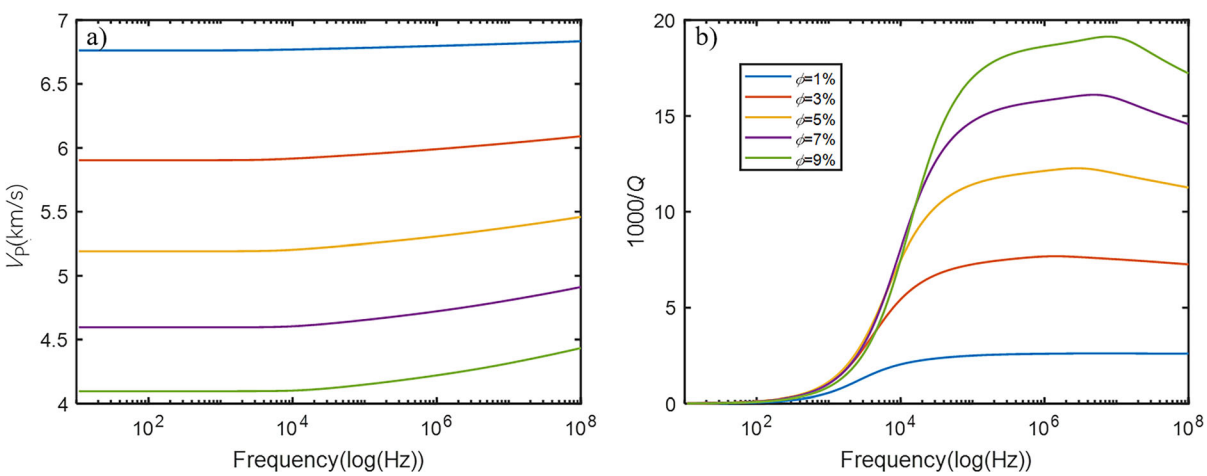

Figure 12
P-wave velocity (**a**) and attenuation (**b**) as a function of frequency and different porosities

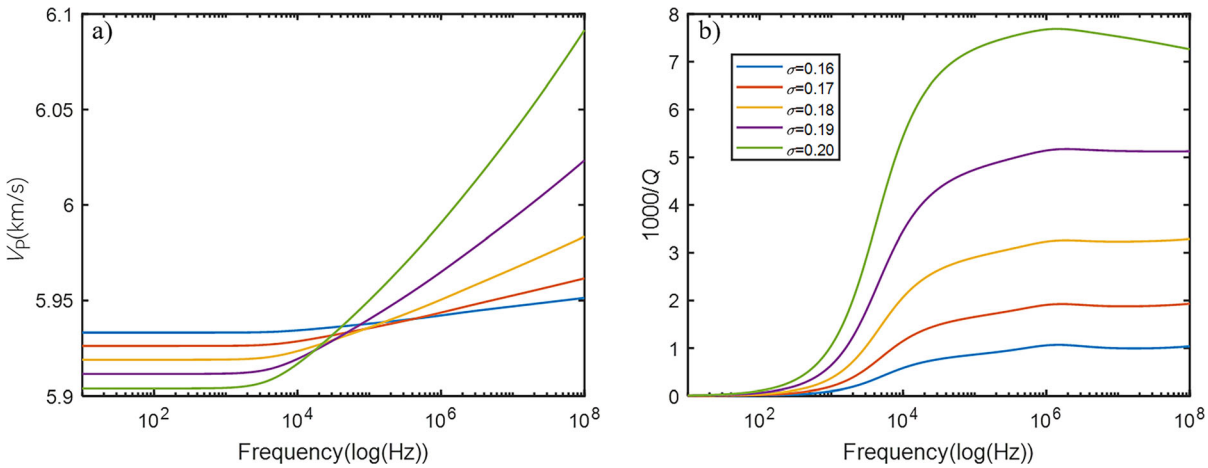

Figure 13
P-wave velocity (**a**) and attenuation (**b**) as a function of frequency and different standard deviations

attenuation increase with increasing porosity, and a slight shift of the relaxation peak towards the high frequency end can be observed. Figure 13 illustrates the velocity and attenuation of the P-wave as a function of frequency at different standard deviations. The porosity is 3%, and the anelasticity increases with increasing standard deviation, while the relaxation peak shifts slightly towards the high frequency range. This is related to the content of microcracks in rock, which increases with increasing standard deviation.

5. Multiscale Rock Physics Templates and Estimation of Reservoir Properties

5.1. RPT at the Ultrasonic Frequency Range

The rock physics template is created based on the modeling procedure as is shown in Fig. 14, where the porosity is between 1 and 6%, the standard deviation is between 0.145 and 0.20, and the mean aspect ratio is between 0.0288 and 0.0363. The colorbar indicates the porosity, and the black, red and blue isolines correspond to the constant mean aspect ratio, standard deviation and total porosity, respectively. In the

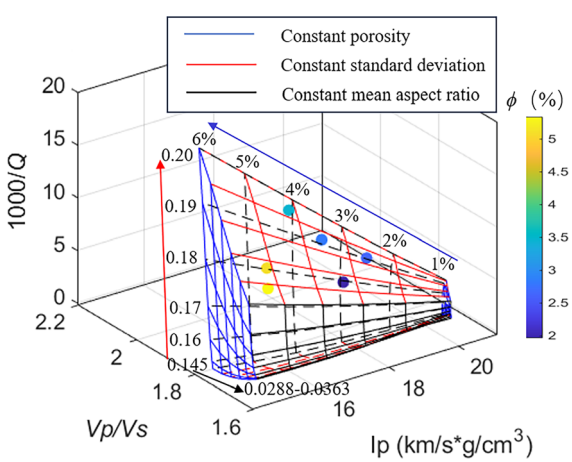

Figure 14
3D RPT at 1 MHz and ultrasonic data (scatters)

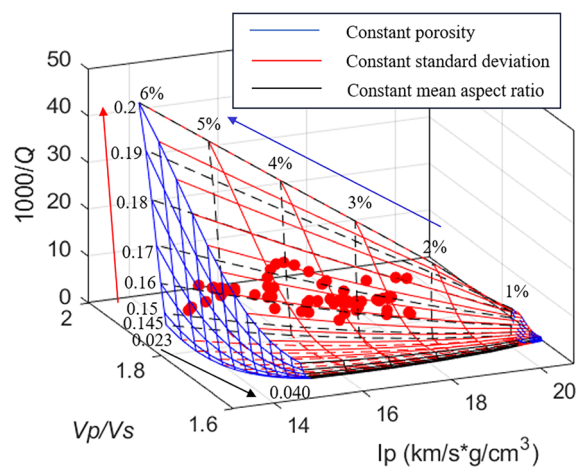

Figure 15
3D RPT at 35 Hz and seismic data (scatters)

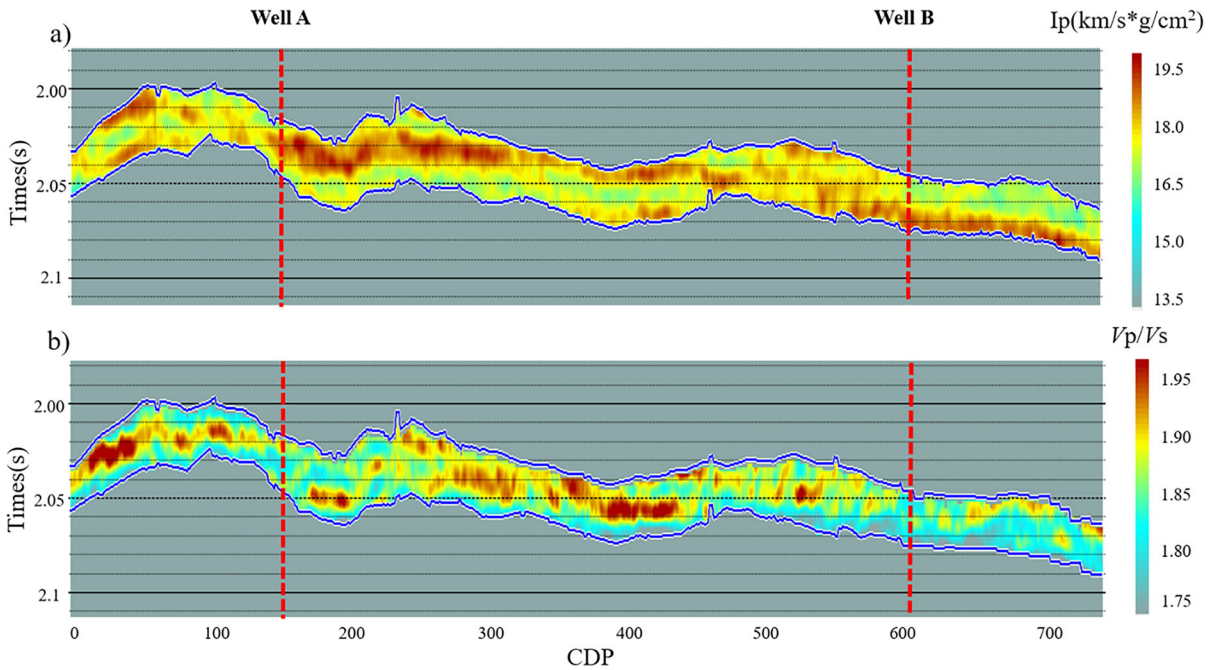

Figure 16
Inversion of a 2D seismic line 1 crossing wells A and B for **a** P-wave impedance and **b** V_P/V_S

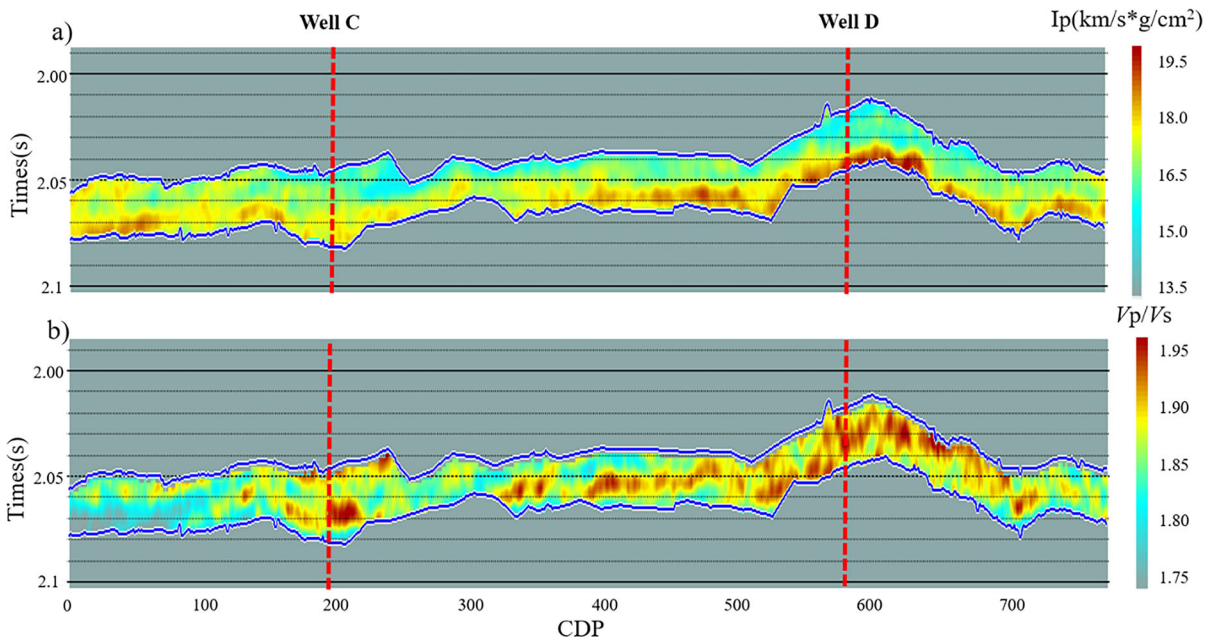

Figure 17
Inversion of a 2D seismic line 2 crossing wells C and D for **a** P-wave impedance and **b** V_P/V_S

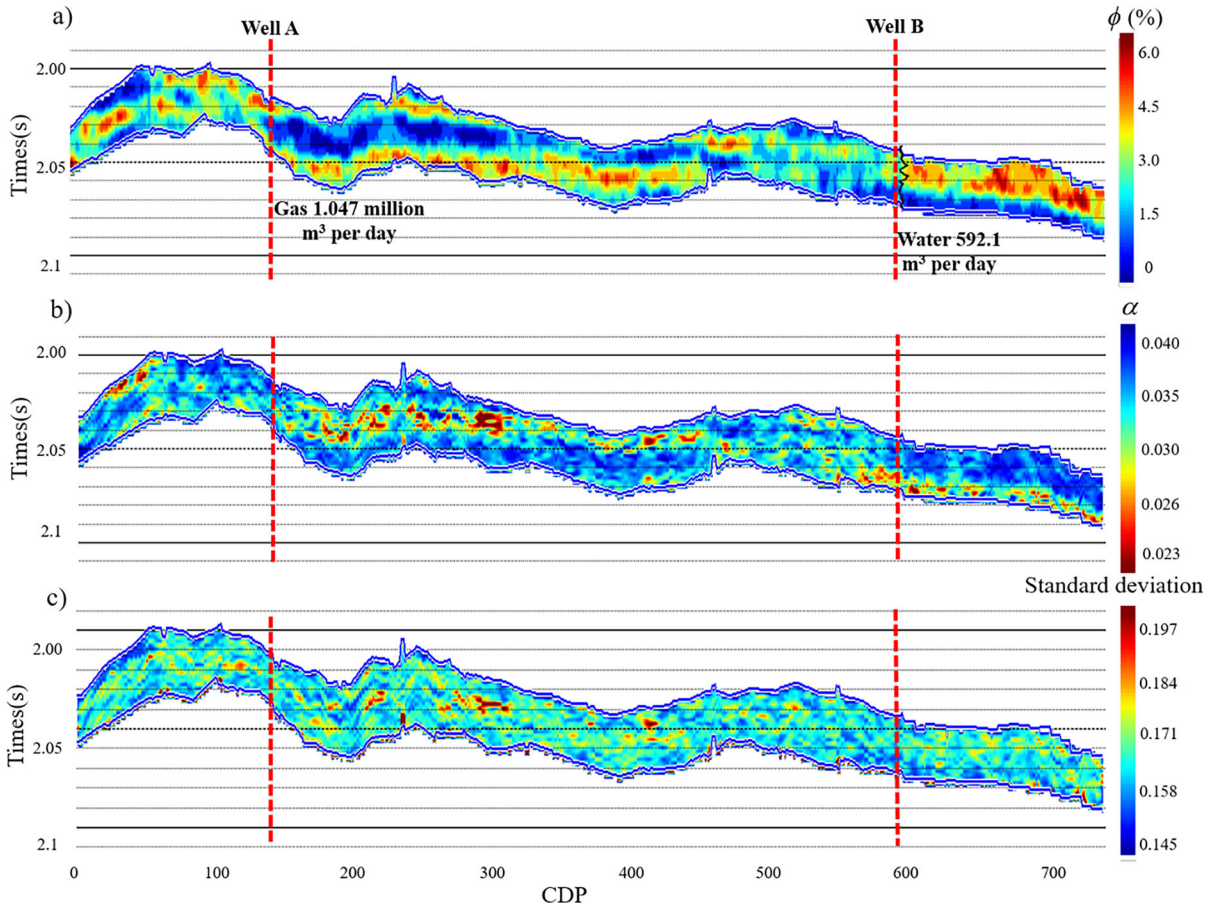

Figure 18
a Porosity, **b** mean aspect ratio and **c** standard deviation profiles of line 1

ultrasonic frequency range, the attenuation of the P-waves and V_P/V_S increase with porosity, while the impedance of the P-waves (Ip) shows the opposite trend. P-wave attenuation and V_P/V_S decrease with increasing mean aspect ratio, and P-wave impedance is opposite. V_P/V_S, P-wave attenuation and P-wave impedance increase with standard deviation. It is also shown that the porosity isolines of the template are essentially consistent with the measured data (scatters).

5.2. *RPT at Seismic Frequency Range*

Figure 15 shows the RPT of the seismic band, where the porosity is in the range of 1–6%, the standard deviation in 0.145–0.20, and the mean aspect ratio in 0.023–0.040. The seismic data are used to obtain the attenuation with the enhanced frequency shift method, and Ip and V_P/V_S are obtained based on the pre-stack seismic inversion (Guo et al., 2023; Nie et al., 2004). The attenuation, Ip and V_P/V_S of the seismic traces around the wells in the work area are considered in the calibration of the template. The variation trends of attenuation, Ip and V_P/V_S in terms of porosity, mean aspect ratio and standard deviation are consistent with those of the ultrasonic frequency domain. The data scatters are distributed within the range of the template.

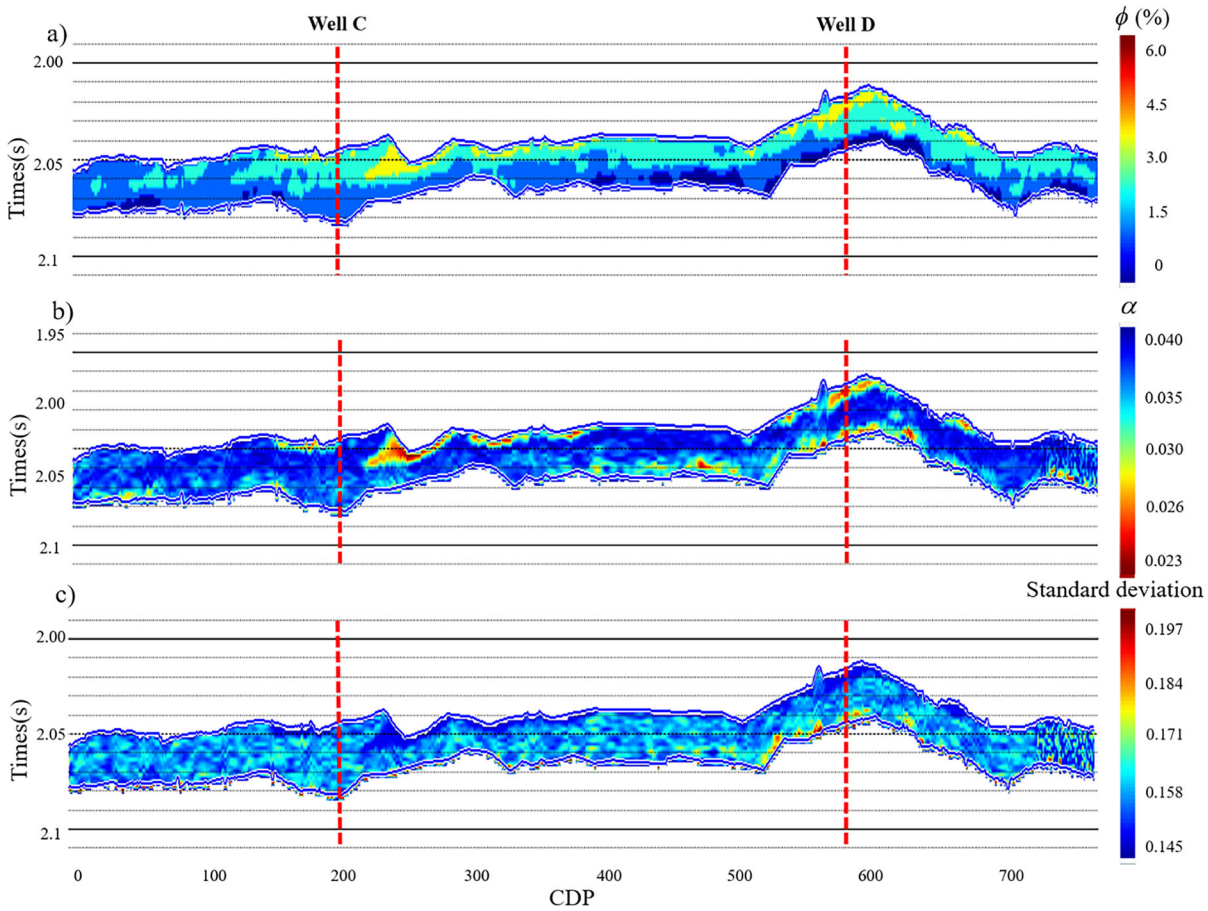

Figure 19
a Porosity, **b** mean aspect ratio and **c** standard deviation profiles of line 2

5.3. Estimation of Reservoir Properties from the Seismic Data

The porosity and pore structure of the reservoirs are estimated for the two lines. Figures 16 and 17 show the inversion profiles of Ip and V_P/V_S for lines 1 and 2. Within the RPT, the grid point on the template closest to the data scatter (Ip, V_P/V_S and attenuation) is considered and thus the porosity, mean aspect ratio and standard deviation are determined. The results are showed in Figs. 17 and 18.

Figure 18 shows the 2D estimated profiles of porosity, mean aspect ratio and standard deviation of the Line 1 dolomite reservoirs. The porosity is generally less than 6%, indicating that the rocks in the formation are tight with low porosity. Wells A and B both show relatively good porosity potential and similar results for the mean aspect ratio. The larger standard deviation indicates larger variations in porosity and microcrack aspect ratio, so the well A with a larger deviation and lower mean aspect ratio may reflect the more developed microcrack system, which is consistent with the results in Fig. 10. Well A's gas production report indicates 1.047 million cubic meters per day, while Well B produces 592.1 cubic meters of water per day (although no good gas production is given for well B, the fluid reserve capacity potential is found here). The predicted porosity, mean aspect ratio and deviations are consistent with the actual production status of the two wells, indicating the potential of reservoir connectivity and fluid storage capacity. The porosity log curve of well B is also indicated in the seismic

profile, which shows the consistency. The gas-bearing dolomite is mainly developed in the upper part of the Longwangmiao Formation. The dolomite is discontinuous and shows large lateral variations in thickness. The result of the prediction is consistent with the geological recognition of the formation (He et al., 2019).

Figure 19 shows the results of the porosity, mean aspect ratio and standard deviation of the line 2 reservoirs. The porosity range is between 0 and 4%. Compared to wells A and B, wells C and D exhibit even lower porosity, a larger mean aspect ratio and a smaller standard deviation, indicating that variations in aspect ratios may be greater in wells A and B than those in wells C and D, and that microcracks are less developed in wells C and D. Based on the analysis in Fig. 10, this is due to the smaller fluctuations and larger mean aspect ratios for stiffer pores/microcracks. According to the production reports, wells C and D provides no evident fluid production.

6. Conclusions

Based on XRD, CTS and ultrasonic experiments, the rock physical properties and pore structure of the dolomite reservoirs of the Longwangmiao formations of the Gaoshiti-Moxi area, Sichuan Basin, are analyzed. To predict the pore structure, it is assumed that the aspect ratio and volume fraction of pores and microcracks follow a statistically normal distribution. The wave properties are simulated based on the effective differential medium and infinituple-porosity theories. P-wave attenuation, impedance and phase velocity ratio are used to create multiscale 3D rock physics templates. The spectral ratio method is used to estimate the P-wave attenuation based on ultrasonic measurements. Seismic wave responses are estimated with the frequency shift method and seismic prestack inversion. The laboratory and seismic data are then used to calibrate the templates for estimating the in-situ reservoir properties.

The estimations show that the overall porosity is generally low, but the microcrack system may be well developed, which is consistent with the actual geologic characteristics of the tight dolomite reservoirs in the target formations. The porosity prediction based on seismic data around one of the wells (well B) is consistent with the log data. The inversion results of standard deviation, mean aspect ratio and porosity can effectively reflect the state of fluid production in the wells. We assume that the pore structure follows a normal distribution, estimate the pore structure by predicting the parameters of the normal distribution and validate it by experiments and actual gas production. This study shows that it is possible to represent the pore structure of rock with a normal distribution. The proposed rock-physics model is capable of providing technical support for estimating the pore structure and guidance for the further reservoir engineering applications.

Acknowledgements

This work is supported by the CNPC Basic Research Project for the 14th Five-Year Plan (2021DJ3502), the National Natural Science Foundation of China (41974123 and 41704109), and the Jiangsu Province Science Fund for Distinguished Young Scholars (BK20200021).

Author Contributions JB: methodology, supervision, modeling, writing-reviewing and funding acquisition. ZA: methodology, modeling, writing and draft preparation. JC: modeling, writing-reviewing and suggestion. MP: software, validation, editing and writing. XY: data collection and analysis. XC: material preparation and validation. All authors contributed to the article and approved the submitted version.

Funding

The CNPC Basic Research Project for the 14th Five-Year Plan, 2021DJ3502, the National Natural Science Foundation of China, 41974123 and 41704109, the Jiangsu Province Science Fund for Distinguished Young Scholars, BK20200021.

Data Availability

No datasets were generated or analysed during the current study.

Declarations

Conflict of interest The authors declare no competing interests.

Publisher's Note Springer Nature remains neutral with regard to jurisdictional claims in published maps and institutional affiliations.

References

Amalokwu, K., Best, A. I., Sothcott, J., Chapman, M., Minshull, T., & Li, X. Y. (2014). Water saturation effects on elastic wave attenuation in porous rocks with aligned fractures. *Geophysical Journal International, 197*(2), 943–947. https://doi.org/10.1093/gji/ggu076

Ba, J., Carcione, J. M., Cao, H., Du, Q. Z., Yuan, Z. Y., & Lu, M. H. (2012). Velocity dispersion and attenuation of P waves in partially-saturated rocks: wave propagation equations in double-porosity medium. *Chinese Journal of Geophysics, 55*(1), 219–231. https://doi.org/10.6038/j.issn.0001-5733.2012.01.021. in Chinese.

Ba, J., Carcione, J. M., & Nie, J. (2011). Biot-Rayleigh theory of wave propagation in double-porosity media. *Journal of Geophysical Research, 116*, B06202. https://doi.org/10.1029/2010JB008185

Ba, J., Xu, W., Fu, L. Y., Carcione, J. M., & Zhang, L. (2017). Rock anelasticity due to patchy-saturation and fabric heterogeneity: A double-double porosity model of wave propagation. *Journal of Geophysical Research: Solid Earth, 122*(3), 1949–1976. https://doi.org/10.1002/2016JB013882

Benaafi, M., Hariri, M., Bertotti, G., Al-Shaibani, A., Abdullatif, O., & Makkawi, M. (2019). Natural fracture system of the Cambro-Permian Wajid Group, Wadi Al-Dawasir, SW Saudi Arabia. *Journal of Petroleum Science and Engineering, 175*, 140–158. https://doi.org/10.1016/j.petrol.2018.12.022

Berryman, J. G. (1992). Single-scattering approximations for coefficients in Biot's equations of poroelasticity. *Acoustical Society of America Journal, 91*, 551–571. https://doi.org/10.1121/1.402518

Cao, Z. N., Li, X. Y., Liu, J., Qin, X. L., Sun, S. H., Li, Z. J., & Cao, Z. Y. (2018). Carbonate fractured gas reservoir prediction based on P-wave azimuthal anisotropy and dispersion. *Journal of Geophysics and Engineering, 15*(5), 2139–2149. https://doi.org/10.1088/1742-2140/aabe58

Carcione, J. M. (2022). *Wavefields in real media. Theory and numerical simulation of wave propagation in anisotropic, anelastic, porous and electromagnetic media* (4th ed.). Elsevier.

Carcione, J. M., & Picotti, S. (2006). P-wave seismic attenuation by slow-wave diffusion: Effects of inhomogeneous rock properties. *Geophysics, 71*(3), O1–O8. https://doi.org/10.1190/1.2194512

Chapman, S., Tisato, N., Quintal, B., & Holliger, K. (2016). Seismic attenuation in partially saturated Berea sandstone submitted to a range of confining pressures. *Journal of Geophysical Research: Solid Earth, 121*(3), 1664–1676. https://doi.org/10.1002/2015JB012575

Dutilleul, J., Bourlange, S., Géraud, Y., & Stemmelen, D. (2020). Porosity, pore structure, and fluid distribution in the sediments entering the northern Hikurangi margin, New Zealand. *Journal of Geophysical Research: Solid Earth, 125*(11), e2020JB020330. https://doi.org/10.1029/2020JB020330

Fan, T. Y., Jiang, L., Nie, Q., Zhao, W. T., Wu, Y., Geng, C., Zhou, X., & Li, T. (2021). Evaluation on development potential in the Lower Cambrian Longwangmiao Formation, Gaoshiti block, Anyue gasfield, Sichuan Basin. *Natural Gas Exploration and Development, 44*(2), 12. https://doi.org/10.12055/gaskk.issn.1673-3177.2021.02.006

Fang, C. N., Pan, B. Z., Wang, Y. H., Rao, Y., Guo, Y. H., & Li, J. L. (2019). Pore-scale fluid distributions determined by NMR spectra of partially saturated sandstones. *Geophysics, 84*(3), MR107–MR114. https://doi.org/10.1190/geo2018-0286.1

Fu, B. Y., Guo, J. X., Fu, L. Y., Glubokovskikh, S., Galvin, R. J., & Gurevich, B. (2018). Seismic dispersion and attenuation in saturated porous rock with aligned slit cracks. *Journal of Geophysical Research, 123*(8), 6890–6910. https://doi.org/10.1029/2018JB015918

Gassmann, F. (1951). Über die elastizität poröser medien. *Vierteljahrsschrift Der Naturforschenden Gesellschaft in Zurich, 96*, 1–23.

Ghanizadeh, A., Clarkson, C. R., Aquino, S., Ardakani, O. H., & Sanei, H. (2015). Petrophysical and geomechanical characteristics of Canadian tight oil and liquid-rich gas reservoirs: Pore network and permeability characterization. *Fuel, 153*, 664–681. https://doi.org/10.1016/j.fuel.2015.03.020

Guo, M. Q., & Fu, L. Y. (2006). Stress associated coda attenuation from ultrasonic waveform measurements. *Geophysical Research Letters, 34*(9), L09307. https://doi.org/10.1029/2007GL029582

Guo, M. Q., Fu, L. Y., & Ba, J. (2009). Comparison of stress associated coda attenuation and intrinsic attenuation from ultrasonic measurements. *Geophysical Journal International, 178*(1), 447–456. https://doi.org/10.1111/j.1365-246X.2009.04159.x

Guo, Q., Ba, J., & Luo, C. (2023). Seismic rock-physics linearized inversion for reservoir-property and pore-type parameters with application to carbonate reservoirs. *Geoenergy Science and Engineering*. https://doi.org/10.1016/j.geoen.2023.211640

Guo, Z. Q., Qin, X. Y., Zhang, Y. M., Niu, C., Wang, D., & Ling, Y. (2021). Numerical investigation of the effect of heterogeneous pore structures on elastic properties of tight gas sandstones. *Frontiers in Earth Science*. https://doi.org/10.3389/feart.2021.641637

Gurevich, B., & Carcione, J. M. (2022). Attenuation and dispersion of elastic waves in porous rocks: Mechanisms and models. *Society of Exploration Geophysicists*. https://doi.org/10.1190/1.9781560803911

He, W., Hao, J., Yang, J., Guan, X., Dai, R., & Li, Y. (2019). Application of pre-stack simultaneous inversion to predict gas-bearing dolomite reservoir: A case study from Sichuan basin, china. *Carbonates and Evaporites., 34*, 1191–1201. https://doi.org/10.1007/s13146-019-00491-6

Hill, R. (1952). The elastic behaviour of a crystalline aggregate. *Proceedings of the Physical Society, 65*, 349–354. https://doi.org/10.1088/0370-1298/65/5/307

Hu, C. H., Tu, N., & Lu, W. (2013). Seismic attenuation estimation using an improved frequency-shift method. *IEEE Geoscience & Remote Sensing Letters, 10*(5), 1026–1030. https://doi.org/10.1109/LGRS.2012.2227933

Hu, J. H., Sun, R. F., & Zhang, Y. (2020). Investigating the horizontal well performance under the combination of microfractures and dynamic capillary pressure in tight oil reservoirs. *Fuel*. https://doi.org/10.1016/j.fuel.2020.117375

Iwamori, H., Ueki, K., Hoshide, T., Hoshide, T., Sakuma, H., Ichiki, M., Watanabe, T., Nakamura, M., Nakamura, H., Nishizawa, T., Nakao, A., Ogawa, Y., Kuwatani, T., Nagata, K., Okada, T., & Takahashi, E. (2021). Simultaneous analysis of seismic velocity and electrical conductivity in the crust and the uppermost mantle: A forward model and inversion test based on grid search. *Journal of Geophysical Research: Solid Earth*. https://doi.org/10.1029/2021JB022307

Kong, L. Y., Ostadhassan, M., Li, C., & Tamimi, N. (2018). Pore characterization of 3D-printed gypsum rocks: A comprehensive approach. *Journal of Materials Science, 53*(7), 5063–5078. https://doi.org/10.1007/s10853-017-1953-1

Li, C. L., Wang, H. H., Wang, L. G., Kang, Y. M., Hu, K. L., & Zhu, Y. S. (2020). Characteristics of tight oil sandstone reservoirs: a case study from the Upper Triassic Chang 7 Member in Zhenyuan area, Ordos Basin, China. *Arabian Journal of Geosciences*. https://doi.org/10.1007/s12517-019-4964-1

Li, F. Y., Zhou, H. L., Jiang, N., Bi, J. X., & Marfurt, K. J. (2015). Q estimation from reflection seismic data for hydrocarbon detection using a modified frequency shift method. *Journal of Geophysics and Engineering, 12*(4), 577–586. https://doi.org/10.1088/1742-2132/12/4/577

Liu, Q. Y., Li, P., Jin, Z. J., Sun, Y. W., Hu, G., Zhu, D. Y., Huang, Z. K., Liang, X. P., Zhang, R., & Liu, J. Y. (2022). Organic-rich formation and hydrocarbon enrichment of lacustrine shale strata: A case study of Chang 7 Member. *Science China Earth Sciences, 65*(1), 118–138. https://doi.org/10.1007/s11430-021-9819-y

Lu, M. H., Cao, H., Sun, W. T., Yan, X. F., Yang, Z. F., Xu, Y. P., Wang, Z. L., & Ouyang, M. (2019). Quantitative prediction of seismic rock physics of hybrid tight oil reservoirs of the Permian Lucaogou Formation, Junggar Basin, Northwest China. *Journal of Asian Earth Sciences, 178*, 216–223. https://doi.org/10.1016/j.jseaes.2018.08.014

Luo, C., Ba, J., & Guo, Q. (2023). Probabilistic seismic petrophysical inversion with statistical double-porosity Biot-Rayleigh model. *Geophysics, 88*(3), M157–M171. https://doi.org/10.1190/GEO2022-0288.1

Mousavi, M., Prodanovic, M., & Jacobi, D. (2012). New classification of carbonate rocks for process-based pore-scale modeling. *SPE Journal, 18*, 243–263. https://doi.org/10.2118/163073-PA

Nelson, R. (2001). *Geologic analysis of naturally fractured reservoirs*. Elsevier.

Nie, J. X., Ba, J., Yang, D. H., Yan, X. F., Yuan, Z. Y., & Qiao, H. P. (2012). BISQ model based on a Kelvin-Voigt viscoelastic frame in a partially saturated porous medium. *Applied Geophysics, 9*(2), 213–222. https://doi.org/10.1007/s11770-012-0332-6

Nie, J. X., Yang, D. H., & Yang, H. Z. (2004). Inversion of reservoir parameters based on the BISQ model in partially saturated porous media. *Chinese Journal of Geophysics, 47*(6), 1101–1105. https://doi.org/10.1002/cjg2.610. in Chinese.

Pang, M., Ba, J., Carcione, J. M., & Saenger, E. H. (2024). Combined acoustical-electrical modeling for tight sandstones verified by laboratory measurements. *International Journal of Rock Mechanics and Mining Sciences, 176*, 105682. https://doi.org/10.1016/j.ijrmms.2024.105682

Pang, M. Q., Ba, J., Carcione, J. M., Picotti, S., Zhou, J., & Jiang, R. (2019). Estimation of porosity and fluid saturation in carbonates from rock-physics templates based on seismic Q. *Geophysics, 84*(6), M25–M36. https://doi.org/10.1190/geo2019-0031.1

Pang, M. Q., Ba, J., Carcione, J. M., Vesnaver, A., Ma, R. P., & Chen, T. S. (2020). Analysis of attenuation rock-physics template of tight sandstones: Reservoir microcrack prediction. *Chinese Journal of Geophysics, 63*(11), 4205–4219. https://doi.org/10.6038/cjg2020N0178. in Chinese.

Reuss, A. (1929). Calculation of the flow limits of mixed crystals on the basis of the plasticity of monocrystals. *Zeitschrift Für Angewandte Mathematik Und Mechanik, 9*, 49–58.

Sanderson, D. J., & Nixon, C. W. (2015). The use of topology in fracture network characterization. *Journal of Structural Geology, 72*, 55–66. https://doi.org/10.1016/j.jsg.2015.01.005

Sayers, C. M. (2008). The elastic properties of carbonates. *The Leading Edge, 27*, 1020–1024. https://doi.org/10.1190/1.2967555

Shi, J., Zou, Y. R., Cai, Y. L., Zhan, Z. W., Sun, J. N., Liang, T., & Peng, P. A. (2021). Organic matter enrichment of the Chang 7 member in the Ordos Basin: Insights from chemometrics and element geochemistry. *Marine and Petroleum Geology, 135*(3–4), 105404. https://doi.org/10.1016/j.marpetgeo.2021.105404

Solazzi, S. G., Guarracino, L., Rubino, J. G., & Holliger, K. (2019). Saturation Hysteresis effects on the seismic signatures of partially saturated heterogeneous porous rocks. *Journal of Geophysical Research: Solid Earth, 124*(11), 11316–11335. https://doi.org/10.1029/2019JB017726

Song, L. T., Wang, Y., Liu, Z. H., & Wang, Q. (2015). Elastic anisotropy characteristics of tight sands under different confining pressures and fluid saturation states. *Chinese Journal of Geophysics, 58*(9), 3401–3411. https://doi.org/10.6038/cjg20150932. in Chinese.

Sun, H., Duan, L., Liu, L., Fan, W. P., Fan, D. Y., Yao, J., Zhang, L., Yang, Y. F., & Zhao, J. L. (2019). The Influence of microfractures on the flow in tight oil reservoirs based on pore-network models. *Energies, 12*(21), 4104. https://doi.org/10.3390/en12214104

Toksöz, M. N., Johnston, D. H., & Timur, A. (1979). Attenuation of seismic waves in dry and saturated rocks: I—Laboratory Measurements. *Geophysics, 44*, 681–690. https://doi.org/10.1190/1.1440969

Tu, N., & Lu, W. (2009). An improved peak-frequency-shift method for Q estimation. In: Beijing International Geophysical Conference and Exposition.

Voigt, W. (1910). Lehrbuch der Kirstallphysik: Teubner.

Wang, P., Li, J. Y., Chen, X. H., & Wang, B. F. (2020). Joint probabilistic fluid discrimination of tight sandstone reservoirs based on Bayes discriminant and deterministic rock physics modeling. *Journal of Petroleum Science & Engineering*. https://doi.org/10.1016/j.petrol.2020.107218

Wei, Q. Q., Wang, Y., Han, D. H., Sun, M., & Huang, Q. (2021). Combined effects of permeability and fluid saturation on seismic wave dispersion and attenuation in partially-saturated sandstone. *Advances in Geo-Energy Research., 5*(2), 181–190. https://doi.org/10.46690/ager.2021.02.07

Xu, S. Y., & Payne, M. A. (2009). Modeling elastic properties in carbonate rocks. *The Leading Edge, 28*, 66–74. https://doi.org/10.1190/1.3064148

Yang, X. F., Wang, X. Z., Dai, L. C., Xie, J. L., & Luo, W. J. (2015). Sedimentary features of the lower Cambrian Longwangmiao Formation in the central Sichuan Basin. *Lithologic Reservoirs, 27*(1), 95–101. https://doi.org/10.3969/j.issn.1673-8926.2015.01.014

Zhang, J. Y., Luo, W. J., Zhou, J. G., Wang, Y., Tang, S., Luo, B., Pan, L. Y., Ni, C., Gu, M. F., & Li, W. Z. (2015). Main origins of high quality reservoir of Lower Cambrian Longwangmiao Formation in the giant Anyue Gasfield, Sichuan Basin, SW China. *Natural Gas Geoscience, 26*(11), 2063–2074.

Zhang, L., Ba, J., & Carcione, J. M. (2021). Wave propagation in infinituple-porosity media. *Journal of Geophysical Research: Solid Earth.* https://doi.org/10.1029/2020JB021266

Zhang, L., Ba, J., Carcione, J. M., & Wu, C. F. (2022). Seismic wave propagation in partially saturated rocks with a fractal distribution of fluid-patch size. *Journal of Geophysical Research: Solid Earth.* https://doi.org/10.1029/2021JB023809

Zhang, S. X., Zou, C. C., & Peng, C. (2018). Numerical simulation study of anisotropic velocities in fractured-vuggy carbonate reservoirs. *Journal of Geophysics and Engineering, 15*, 1851–1863. https://doi.org/10.1088/1742-2140/aabd3f

Zhao, L. X., Cao, C. H., Yao, Q. L., Wang, Y. R., Li, H., Yuan, H. M., Geng, J. H., & Han, D. H. (2020). Gassmann consistency for different inclusion-based effective medium theories: implications for elastic interactions and poroelasticity. *Journal of Geophysical Research: Solid Earth.* https://doi.org/10.1029/2019JB018328

Zhao, L. X., Qin, X., Han, D. H., Geng, J. H., Yang, Z. F., & Cao, H. (2016). Rock-physics modeling for the elastic properties of organic shale at different maturity stages. *Geophysics, 81*(5), D527–D541. https://doi.org/10.1190/geo2015-0713.1

Zheng, D. Y., Pang, X. Q., Zhou, L. M., You, X. C., Liu, X. H., Guo, F. X., & Li, W. (2020). Critical conditions of tight oil charging and determination of the lower limits of petrophysical properties for effective tight reservoirs: A case study from the Fengcheng Formation in the Fengcheng area, Junggar Basin. *Journal of Petroleum Science and Engineering*. https://doi.org/10.1016/j.petrol.2020.107135

(Received December 30, 2023, revised May 12, 2024, accepted May 16, 2024, Published online May 25, 2024)